Minimal Energy Packings and Collapse of Sticky Tangent Hard-Sphere Polymers

Robert S. Hoy and Corey S. O'Hern

Department of Mechanical Engineering, Yale University, New Haven, Connecticut 06520-8286, USA
and Department of Physics, Yale University, New Haven, Connecticut 06520-8120, USA

(Received 7 May 2010; revised manuscript received 28 June 2010; published 5 August 2010)

We enumerate all minimal energy packings (MEPs) for small single linear and ring polymers composed of spherical monomers with contact attractions and hard-core repulsions and compare them to corresponding results for monomer packings. We define and identify "dividing surfaces" in polymer packings, which reduce the number of arrangements that satisfy hard-sphere and covalent-bond constraints. Compared to monomer MEPs, polymer MEPs favor intermediate structural symmetry. We also examine the packing-preparation dependence for longer single chains using molecular dynamics simulations. For slow temperature quenches, chains form crystallites with close-packed cores. As the quench rate increases, the core size decreases and the exterior becomes more disordered. By examining the contact number, we connect the suppression of crystallization to the onset of isostaticity in disordered packings.

DOI: 10.1103/PhysRevLett.105.068001 PACS numbers: 64.70.km, 45.70.−n, 64.60.Cn, 82.70.Dd

Over the past several decades significant research activity has focused on understanding dense packings of hard spheres, since they serve as model systems for atomic and colloidal liquids and glasses, jammed granular media, and compressed foams and emulsions. An intriguing property of hard-sphere systems is that they can be prepared in crystalline, partially ordered, and amorphous packings [1]. Packings of "sticky" hard spheres with contact attractions have been used to investigate self-assembly of colloidal particles with depletion attractions. Arkus *et al.* recently combined graph theory and geometrical techniques [2,3] to enumerate minimal energy packings (MEPs), i.e., those with the maximum number of contacts, for $N \leq 10$ sticky hard spheres. Their predictions agreed with experiments on attractive colloids [4].

However, there have been few studies of packings of sticky tangent hard-sphere polymers, which can model polymer collapse, protein folding, and protein interactions [5]. Recent simulations [6,7] and experiments [8] have investigated polymer packings; however, they considered nonsticky spheres with only hard-core repulsions, where free volume, not energy, is relevant. Thus, there is little understanding of how covalent-bond and chain uncrossability constraints affect structural and mechanical properties of sticky hard-sphere polymer packings and the probabilities with which these occur.

In this Letter, we perform exact enumeration studies of MEPs for sticky, tangent, monodisperse hard-sphere polymers (both linear and cyclic) and contrast the results with those for sticky hard spheres without polymer constraints. Our studies begin to address several overarching questions. (1) How do the probabilities for obtaining polymer MEPs differ from those for sticky hard-sphere MEPs? (2) How do the properties of single compact polymers depend on collapse dynamics; e.g., do they collapse into crystalline or amorphous clusters?

Our results show that polymer constraints reduce the ways in which hard spheres can be arranged into MEPs, and the strength of this effect varies for different macrostates (i.e., structurally distinct packings). We demonstrate that the large reduction in the number of arrangements may be understood in terms of *dividing surfaces*. These split polymer packings into disjoint regions and eliminate particle-label permutations that do not correspond to polymer chains. We find that polymer MEPs with intermediate structural symmetry are more frequent relative to the monomer case, where entropy favors low symmetry MEPs [4].

In addition, using molecular dynamics (MD) simulations of temperature quenches at various rates $\dot{T}$, we show that single chains display glassy dynamics during collapse, and that the final polymer packings depend on $\dot{T}$. In the slow quench rate limit, the chains undergo a sharp [9] transition to crystallites, with a jump in the energy and number of contacts N_c (including covalent bonds) at temperature $T = T_{\rm melt}$. The crystallites possess a close-packed core surrounded by a "surface" whose size and disorder increase with $|\dot{T}|$. For slow quenches, N_c at $T_{\rm melt}$ jumps from below the minimal number $N_c^{\rm min} = 3N - 6$ required for mechanical stability [11] to $N_c^{\rm slow}$, where a significant fraction of the monomers possess 12 contacts. In the large $|\dot{T}|$ limit, the clusters are disordered with $\lesssim N_c^{\rm min}$ contacts even as $T \to 0$, showing that rigidification can hinder crystallization.

We first describe exact enumeration methods for monomer and polymer MEPs [12]. To generate possible packings for a given number of spheres N and contact number N_c, we iterate over all $N \times N$ adjacency matrices $\bar{A}$ satisfying $\sum_{j>i} A_{ij} = N_c$. The elements of $\bar{A}$ are 1 for contacting particles and 0 for noncontacting particles and diagonal entries. Covalent bonds link sticky spheres to form a polymer chain with length N; $A_{i,i+1} = 1$ for $1 \leq i < N$ for linear chains, and additionally $A_{1,N} = 1$ for

TABLE I. Statistics for MEPs with N spheres and N_c contacts. M is the number of macrostates, f_r, f_p, and f_m are the fraction of microstates obeying minimal rigidity constraints that also satisfy hard-sphere constraints, respectively, for rings, linear polymers, and monomers, and Ω_r, Ω_p, and Ω_m are the total numbers of microstates satisfying both minimal rigidity and hard-sphere constraints. Values for f and Ω do not account for chiral twins [2]. In agreement with [2], we find 1 and 4 floppy macrostates (in the $k \to \infty$ limit [12]), respectively, for $N = 9$ and ($N = 10$, $N_c = 24$). However, we find 2 and 55 more rigid macrostates[*,#] for these cases [12,15]. Adjacency matrices and coordinate solutions for all microstates are available online [16]. $\cdots$ indicates data not available.

N	N_c	M	f_r	f_p	f_m	f_r/f_m	f_p/f_m	Ω_r	Ω_p	Ω_m
5	9	1	1	1	1	1	1	5	6	10
6	12	2	0.435	0.463	0.494	0.88	0.94	34	50	195
7	15	5	0.102	0.114	0.134	0.76	0.85	273	486	5712
8	18	13	1.66×10^{-2}	1.91×10^{-2}	2.45×10^{-2}	0.68	0.78	2668	5500	231 840
9	21	52*	1.40×10^{-3}	2.46×10^{-3}	3.34×10^{-3}	0.42	0.74	30 663	71 350	12 368 160
10	24	278*,#	2.21×10^{-4}	2.55×10^{-4}	$\cdots$	$\cdots$	$\cdots$	426 590	1 093 101	$\cdots$
10	25	3	2.05×10^{-6}	1.98×10^{-6}	$\cdots$	$\cdots$	$\cdots$	5905	12 138	$\cdots$

rings. The distinction between permanent covalent and thermally fluctuating noncovalent bonds is not important for static packings; we include both types in N_c.

We enumerate all adjacency matrices satisfying the above conditions and then identify those that also fulfill hard-sphere and minimal rigidity constraints. Hard-sphere constraints imply that the center-to-center distances r_{ij} between unit spheres i and j obey $r_{ij} \geq 1$, where the equality holds for contacting pairs. Necessary conditions for rigidity are that each monomer possesses at least three contacts and $N_c \geq N_c^{\min}$ [13].

To enforce these constraints, we implemented geometrical rules developed by Arkus *et al.* [2,3] that eliminate invalid adjacency matrices. For the remaining configurations, we solved the system of quadratic equations

$$|\vec{r}_i - \vec{r}_j|^2 = d_{ij}^2 \tag{1}$$

for sphere positions $\vec{r}_i$ to an accuracy of 10^{-9}. We also calculated the dynamical matrix [all second derivatives of the energy in Eq. (2) with respect to monomer displacements] for all configurations, which allowed us to identify rigid (with $3N - 6$ nonzero eigenvalues) and floppy configurations [13] (with fewer nonzero eigenvalues) [12].

From this procedure, we obtain microstates and macrostates for a given N and N_c that satisfy hard-sphere and minimal rigidity constraints and the relevant polymeric constraints. Each macrostate is characterized by an adjacency matrix that is nonisomorphic to and a set of interparticle distances $\{r_{ij}\}$ that is different from those characterizing other macrostates [12]. With this definition, no macrostate can be rotated or reflected such that it yields a different macrostate. Every connected sticky hard-sphere macrostate admits a linear polymer macrostate [14]. Thus, sticky-sphere and linear polymer packings have identical macrostates. We have also verified this for ring packings for $N \leq 10$.

A microstate is a particular labeling of the particles 1 through N that comprise an N-particle macrostate with N_c contacts. Many microstates correspond to each macrostate due to particle permutations for monomer packings [4], and for polymers, the multiple possible paths through a given macrostate. The total number of microstates Ω_m, Ω_p, and Ω_r is given by the sum of microstates for each macrostate for monomers, linear polymers, and rings, respectively [12]. For monomer packings, which lack covalent bonds, the number of microstates for each macrostate (ignoring chirality) is given simply by a geometric factor $\Omega_m^i = P_i$, where P_i is the number of allowed permutations of particle indices for macrostate i [3]. For polymer packings, the number of microstates is not given by this relation since one must ensure that particle indices are consecutive.

Exact enumeration results are displayed in Table I, which shows the number of macrostates M, fraction f of adjacency matrices with N_c contacts obeying minimal rigidity that also satisfy hard-sphere constraints, and Ω_m, Ω_p, and Ω_r for $5 \leq N \leq 10$. f corresponds to the probability to obtain a packing for an ''ideal'' protocol that samples adjacency matrices uniformly. From Table I, we see that f decreases approximately exponentially with N for $N \geq 5$, and even faster for $N > 9$. Part of the reason for the strong decrease in f between $N = 9$ and 10 is the decrease in macrostates from 52 to 3. This occurs because $N = 10$ MEPs possess $N_c = N_c^{\min} + 1$, which exceeds the number of degrees of freedom. Equation (1) is then overconstrained, and its solutions possess special symmetries. The increase in N_c signals the onset of crystal nucleation and the formation of a close-packed core. The ability to enumerate the numbers of isostatic ($N_c = N_c^{\min}$) and hyperstatic ($N_c > N_c^{\min}$) packings will yield insight into systems where glass and crystallization transitions compete.

For the N studied here, hard-sphere constraints are more difficult to satisfy for minimally rigid polymer packings compared to monomer packings: $f_r < f_p < f_m$ [17]. A key mechanism for the reduction in f is the occurrence of ''dividing surfaces'' in polymer packings. A dividing surface is any minimal subset of a connected cluster of contacting monomers that geometrically splits it into two. Any polymer path that traverses a dividing surface that does not also topologically divide the polymer is blocked and invalid. Specifically, if m consecutive monomers

$i+1,\ldots,i+m$ occupy an m-monomer dividing surface S, any polymer path where the sets of monomers J and K divided by S are anything other than $1,2,\ldots,i$ and $i+m+1, i+m+2,\ldots,N$ (or vice versa) is blocked. In other words, any path that starts in J, enters S, and traverses it (passes through all monomers in S) is blocked unless it traverses all monomers in J before entering S. Figure 1(a) schematically depicts the sets J and K and two dividing surfaces for a $N=8$ macrostate. By definition, blocking does not occur in monomer packings.

In Table I, we see that the blocking effect increases sharply with N since f_r/f_m and f_p/f_m decrease significantly. Blocking also reduces [17] the fractions of allowed ring microstates relative to those for linear polymers f_r/f_p since rings do not possess chain ends. Another clear feature in Fig. 1(b) is that blocking changes the relative frequencies with which macrostates of different symmetries are populated. Ring and linear polymer packings are more likely to possess intermediate symmetry than monomer packings, whereas the opposite is true for macrostates with the lowest and highest symmetries. Highly symmetric macrostates possess many distinct blocking surfaces, and low symmetry macrostates possess a surplus of closed trimers as shown in Fig. 1(a).

The enumeration studies illustrate an interesting competition between energy and entropy. For $N \geq 10$, MEPs are overconstrained with $N_c > N_c^{\min}$. This suggests that if the system becomes trapped in a metastable state (e.g., with $N_c = N_c^{\min}$), rearrangements into MEPs will be slow because of their low entropy. Thus, glassy dynamics in single polymer chains should be observable in systems quenched at varying rates. For $k_BT \gg |\epsilon|$, where $-\epsilon$ is the contact energy, polymers adopt random-coil configurations with $N_c \ll N_c^{\min}$. As the polymer is cooled, one expects quench rate effects to become important when $N_c \simeq N_c^{\min}$ [18].

To demonstrate glassy dynamics for single linear polymer chains, we employ MD simulations in which monomers interact via the potential energy

$$U_{\text{harm}}(r) = \begin{cases} -\epsilon + \frac{k}{2}(\frac{r}{D}-1)^2 & r < r_c \\ 0 & r > r_c, \end{cases} \quad (2)$$

where k is the spring constant and $D=1$ is the monomer diameter. The temperature T is controlled via a Langevin thermostat. The unit of time is $\tau = \sqrt{mD^2/\epsilon}$, where m is the monomer mass. The cutoff radius $r_c/D = \infty$ for covalently bonded monomers and $1+\sqrt{2\epsilon/k}$ for noncovalently bonded monomers. U_{harm} reduces to the energy for tangent sticky hard spheres [19] in the limit $k \to \infty$ and possesses the same MEPs. For $N \leq 10$, the MEPs from

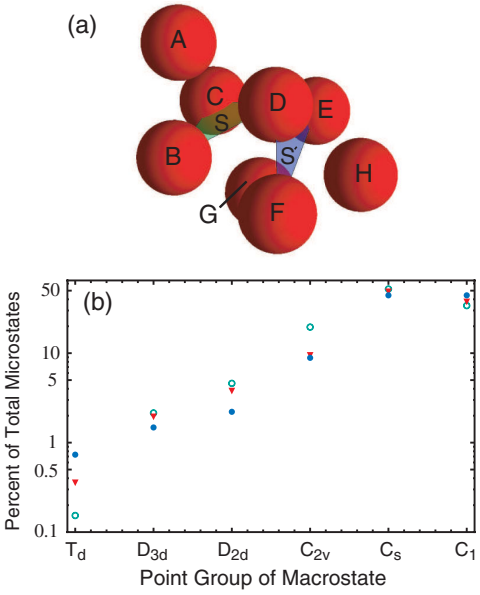

FIG. 1 (color online). (a) Schematic of dividing surfaces S and S' [colored triangles formed by monomers (B, C, D) and (D, E, F), respectively] for an $N=8$ macrostate. For S, region J consists of monomer A and region K of monomers (E, F, G, H), or vice versa. (b) Fraction of microstates for packings from each symmetry group for cyclic (open circles) and linear (downward triangles) polymers and monomers (filled circles) with $N=8$. Results in (b) do not account for chiral structures.

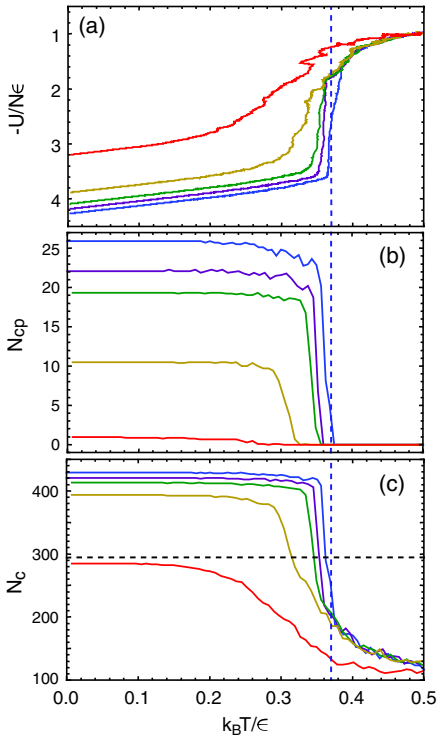

FIG. 2 (color online). (a) Potential energy per particle $(-U/N\epsilon)$, (b) number of particles with 12 contacts (N_{cp}), and (c) total number of contacts (N_c) versus k_BT/ϵ for single linear polymers with $N=100$ at different quench rates. Data [top to bottom, (b),(c); bottom to top, (a)] are for quench rates $k_B\dot{T}\tau/\epsilon = -10^{-3}$, -10^{-4}, -10^{-5}, -10^{-6}, and -10^{-7}. The critical quench rates are $|k_B\dot{T}^*/\epsilon| \sim 10^{-7}/\tau$ and $|k_B\dot{T}^{**}/\epsilon| \sim 10^{-3}/\tau$. All results are averaged over several independent initial configurations. The horizontal (vertical) dotted lines indicate $N_c = N_c^{\min}$ $(k_BT/\epsilon = 0.37)$.

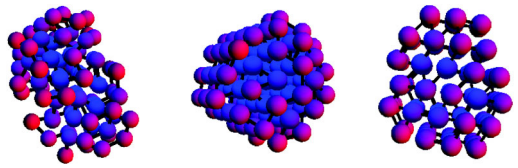

FIG. 3 (color online). Collapsed structures at $T = 0$ for a single $N = 100$ linear polymer using two quench rates: $k_B\dot{T}\tau/\epsilon = -10^{-4}$ (left) and -10^{-7} (middle, right). The packing in the right-hand panel is rotated compared to that in the middle panel to show its hexagonal planes.

simulations agree with those from complete enumeration for $k \gtrsim 1600\epsilon$ ($r_c \lesssim 1.04D$).

Figure 2(a) shows the potential energy per particle $-U/N\epsilon$ for different quench rates $\dot{T}$. At low $\dot{T}$, a sharp transition between coils and crystallites [9,10] is observed at $T_{\text{melt}} \simeq 0.37\epsilon/k_B$. The crystallites consist of a close-packed core with N_{cp} monomers (each with 12 contacts) and a less-ordered exterior. The crystallization transition coincides [Fig. 2(b)] with a sharp transition in N_{cp}, which implies a change of symmetry within the core, from liquid-like to close packed.

At higher rates, the dynamics becomes glassy near T_{melt}, and the systems do not approach the ground state energy even as $T \to 0$. We associate the suppression of crystallization with the onset of rigidity. Evidence for this is given in Fig. 2(c). The data show two ''critical'' quench rates: $\dot{T}^*$ and $\dot{T}^{**}$. For $|\dot{T}| < |\dot{T}^*|$, the jump in N_c and N_{cp} resembles a first-order transition. For $|\dot{T}| > |\dot{T}^{**}|$, the systems do not form minimally rigid clusters even at $T = 0$. Even though the critical rates and T_{melt} are N dependent, the trends are clear. For $N = 100$ systems, we estimate $|k_B\dot{T}^*/\epsilon| \sim 10^{-7}/\tau$ and $|k_B\dot{T}^{**}/\epsilon| \sim 10^{-3}/\tau$.

The effects of quench rate on end states of quenches to $T = 0$ are visualized in Fig. 3. Monomers are color-coded by the number of contacts: dark blue (red) [dark gray (light gray)] indicates close packing ($\ll$12 contacts). The left-hand panel shows a typical configuration after a fast quench with $k_B\dot{T} = -10^{-4}\epsilon/\tau$; we see a small close-packed core surrounded by a disordered exterior. The middle and right-hand panels show a collapsed structure at $T = 0$ from a slow quench ($k_B\dot{T} = -10^{-7}\epsilon/\tau$). The close-packed core is much larger, and the exterior is more crystalline. The large gaps visible in the rightmost panel indicate the order is (stack-faulted) hcp [20].

We examined minimal energy packings of sticky tangent hard-sphere linear and cyclic polymers, and compared them to monomer packings for small N. The packings are the same, but polymer packings possess significantly smaller entropies compared to monomer packings due to dividing surfaces, which arise from covalent-bond constraints. Entropic suppression via blocking is strongest for structures of both very high and low symmetry. In both monomer and polymer cases, the fraction of states satisfying hard-sphere constraints decreases at least exponentially with increasing N, and faster when $N_c > N_c^{\min}$.

We also performed MD simulations of single linear chains with larger N, which link glassy dynamics to the onset of rigidity. This work sets the stage for future studies that investigate whether cooperative dynamics from chain connectivity and uncrossability constraints improves or impedes the glass-forming ability of single polymers compared to colloidal systems.

We thank V. N. Manoharan for helpful discussions. Our results were obtained using the Boost Graph Library, a modified version of Arkus' structure solver [3], and LAMMPS [21]. Support from NSF Grant No. DMR-0835742 is gratefully acknowledged.

[1] C. S. O'Hern, L. E. Silbert, A. J. Liu, and S. R. Nagel, Phys. Rev. E **68**, 011306 (2003).
[2] N. Arkus, V. N. Manoharan, and M. P. Brenner, Phys. Rev. Lett. **103**, 118303 (2009).
[3] N. Arkus, Ph.D. thesis, Harvard University, 2009.
[4] G. Meng, N. Arkus, M. P. Brenner, and V. N. Manoharan, Science **327**, 560 (2010).
[5] T. T. Pham, M. Bajaj, and J. R. Prakash, Soft Matter **4**, 1196 (2008); M. J. Behe, E. E. Lattman, and G. D. Rose, Proc. Natl. Acad. Sci. U.S.A. **88**, 4195 (1991); L. Lo Conte, C. Chothia, and J. Janin, J. Mol. Biol. **285**, 2177 (1999).
[6] M. Laso, N. C. Karayiannis, K. Foteinopoulou, M. L. Mansfield, and M. Kröger, Soft Matter **5**, 1762 (2009); N. C. Karayiannis, K. Foteinopoulou, and M. Laso, Phys. Rev. E **80**, 011307 (2009).
[7] L. M. Lopatina, C. J. O. Reichhardt, and C. Reichhardt, arXiv:0912.1874.
[8] L.-N. Zou *et al.*, Science **326**, 408 (2009).
[9] It cannot be rigorously classified as first order since $N = 100$ chains are far from the thermodynamic limit [10].
[10] M. P. Taylor, W. Paul, and K. Binder, J. Chem. Phys. **131**, 114907 (2009); Phys. Rev. E **79**, 050801 (2009).
[11] A. Donev, S. Torquato, and F. H. Stillinger, Phys. Rev. E **71**, 011105 (2005).
[12] See supplementary material at http://link.aps.org/supplemental/10.1103/PhysRevLett.105.068001 for additional details of the exact enumeration methods and rigidity analyses.
[13] D. J. Jacobs and M. F. Thorpe, Phys. Rev. Lett. **75**, 4051 (1995).
[14] T. Biedl *et al.*, Discrete Comput. Geom. **26**, 269 (2001).
[15] For $N = 10$, $N_c = 24$, there are 279 macrostates; we list the 278 that cannot be formed by breaking one contact of a $N = 10$, $N_c = 25$ state [3].
[16] http://ml313h.eng.yale.edu/~robhoy/MEPs.tar.
[17] Except for ($N = 10$, $N_c = 25$); the slight difference may correspond to suppression of $\bar{A}$'s not satisfying minimal rigidity constraints.
[18] A. Huerta and G. G. Naumis, Phys. Rev. B **66**, 184204 (2002).
[19] S. B. Yuste and A. Santos, Phys. Rev. E **48**, 4599 (1993).
[20] N. C. Karayiannis, K. Foteinopoulou, and M. Laso, Phys. Rev. Lett. **103**, 045703 (2009).
[21] S. Plimpton, J. Comput. Phys. **117**, 1 (1995).